PbS/IGZO hybrid structure photo-field-effect transistor with high performance

Ying Meng[1,2,3], Jiawei Wang[1,2] ✉, Anjie Ming[1,2], Yinghui Wang[1,2,3], Xuewen Shi[1,2], Molin Li[4], Weibing Wang[1,2], Ling Li[1,2]

[1]*Department of Microelectronics, University of Chinese Academy of Sciences, Beijing 100029, People's Republic of China*
[2]*Institute of Microelectronics Chinese Academy of Sciences, Beijing 100029, People's Republic of China*
[3]*Kunshan Branch, Institute of Microelectronics Chinese Academy of Sciences, Kunshan, Jiangsu 215347, People's Republic of China*
[4]*National Center for Nanoscience and Technology, Beijing 100190, People's Republic of China*
✉ *E-mail: wangjiawei@ime.ac.cn*

Published in Micro & Nano Letters; Received on 30th May 2018; Revised on 25th September 2018; Accepted on 11th October 2018

To optimise the performance of photo-field-effect transistor, a back-gate hybrid structure was developed. In this hybrid phototransistor, lead sulphide (PbS) thin film was prepared using physical vapour deposition as a photosensitive layer. Discontinuous and uniform PbS film was obtained by controlling the deposition rate and time of PbS powders. Amorphous indium gallium zinc oxide (IGZO) with high mobility was used as an active layer. In this work, The hybrid structure phototransistor shows an excellent performance: device mobility (μ) reach 8.7 $cm^2V^{-1}s^{-1}$, and responsivity achieve 2.7×10^4 A/W in visible spectrum and 5.7 A/W in near-infrared spectrum, respectively. Furthermore, the transistor exhibits detectivity up to 2.79×10^{13} $cmHz^{1/2}W^{-1}$. The device also exhibits characteristics of the ideal diode: the saturation current of the diode is as small as 0.422 nA, and the responsivity of diode is ~0.74 A/W. Simplified manufacturing processes effectively reduce the cost of fabricated device and provide better device stability.

1. Introduction: Optoelectronic thin film transistor (TFT) is an important fundamental component in various applications, including smart wearable products [1], lightweight sheet image scanner [2], remote sensing [3], active-matrix flat-panel displays [4], environmental monitoring [5] and memory devices [6]. Amorphous indium gallium zinc oxide (IGZO) which exhibits electron mobility as high as 10–50 $cm^2V^{-1}s^{-1}$, good transparency and applicability for the low-temperature process has potential to serve as active layer in TFT [7, 8]. However, the large optical bandgap (3.2 eV) has limited its response to light of wavelength >420 nm [4]. To enhance the sensing ability of the IGZO device in the visible region, TFT with heterojunction structure is proposed. II–VI compounds are widely applied in optoelectronics for producing various radiation transistors, such as molybdenum disulphide (MoS_2) [9], lead sulphide (PbS) [10] and lead selenide (PbSe) [11]. Among the materials, PbS contributes to the advantages of high light absorption coefficient, simple amplifier circuit and good performance at room temperature [12]. PbS can also broaden the detection spectrum since it is a direct bandgap semiconductor with an exciton radius of 18 nm, and has the narrow bandgap of 0.37 eV [13]. So, PbS was chosen as a light absorber because it can easily overcome the IGZO wavelength limitation in the ultraviolet region and extend the detection spectrum to the visible region or even the near infrared.

In this Letter, a new method to fabricate PbS/IGZO hybrid structure phototransistors was designed. The IGZO TFT was covered with PbS. To form discontinuous photosensitive film, physical vapour deposition (PVD) was used to prepare PbS nano-grains with a size of about 40 nm. The process of discontinuous PbS thin film as photosensitive layer is more stable and easier to be prepared than the solution gel method for quantum dot. The phototransistor has high responsivity using interdigital comb structure with high width-to-length ratio as source and drain electrodes. The electrical and optical properties of phototransistors and diode characteristics were analysed. The phototransistor presents better performance than most of the other TFTs based on IGZO and other PbS quantum dot phototransistors, while keeping well gate tunable ability.

2. Experimental: First, heavily doped p-type silicon wafer was thermally oxidised as a gate dielectric layer with a thickness of 300 nm. Then, amorphous IGZO (Ga_2O_3: In_2O_3: ZnO = 1:1:1) worked as active layers with thickness of 30 nm, which were synthesised by vacuum magnetron sputtering with power of 80 W, pressure of 3 mTorr and argon flow rate of 20 sccm. The photosensitive layer was composed of the discontinuous PbS thin film, which was formed by PVD. The PbS powder was thermally evaporated into vapour molecules, and then the molecules self-assembled into single crystalline nanoparticles with thickness of 1 nm. The Au/Ti source/drain electrodes were employed by electron beam lithography and patterned by conventional lift-off process, which prepared with thickness of 10 nm Ti and 80 nm Au, respectively. The source/drain electrodes were used to define the channel width of 60 μm and length of 2 μm. The electrodes were designed to interdigital comb structure.

The particle size and deposition state of PbS were characterised by atomic force microscope (AFM). The microstructure and size of source/drain electrodes were observed by Olympus microscope imaging system and scanning electron microscope (SEM). The electrical and optical-electrical properties of the devices were characterised using a Keithley 4200 semiconductor analyser in a TTP4 probe station (Lake Shore) under vacuum with pressure of 1.1×10^{-4} Torr. To verify the optical response, a laser with wavelength of 532 and 808 nm were used as light sources to characterise the transistor performance. A full wavelength spectrum halogen lamp was applied to characterise the diode performance.

3. Results and discussions: PbS thin film has a very narrow bandgap, therefore it responds well to light both in visible light and in the near-infrared band. The electron in the semiconductor valence band absorbs the photon energy, after that transferring into the conduction band which inducing intrinsic absorption. The conductivity of the semiconductor changes owing to the generation of photo-generated free electrons in the conduction band and the photo-generated free holes in the valence band [14]. The energy band was bending due to efficient charge transfer from low potential to high potential. The band diagram of active layer and the

light-sensitive layer was shown in Fig. 1. The electron transition occurs from valence band to conduction band as the wavelength $\lambda \geq 1.24/E_g$ (μm). The photo-generated carriers, both holes and electrons, would be collected by source and drain electrodes. By colliding with the crystal lattice, the photo-generated electrons lose excess energy in the form of emitted photons in a very short time and become heat-balanced electrons. The electron transport rate of transistor in the charge transport layer could reach high velocity due to the high mobility of IGZO and the high aspect ratio of source and drain electrodes.

3.1. Morphological and structure properties: Fig. 2*a* shows the microstructure image of the single transistor. The single finger with width-to-length ratio of 30 (W/L = 60 μm/2 μm).

Fig. 2*b* shows the top surface SEM with channel length 1.507 μm. The electrode channels which prepared by lift-off patterning are slightly smaller than the design, which may be due to the shorter lithographic exposure time. A smaller channel length is exactly more conducive to increase the saturation current of the device. In addition, a small grain size film with a low nucleation density was obtained through a slow deposition rate (0.02 nm/s). According to Fig. 3, the particles size of sample is ~20–60 nm, and they are staggered to form a discontinuous light-sensitive film. Due to the discontinuity of the PbS film, IGZO with high mobility can be ensured as carrier transport layer.

3.2. TFT electrical properties: Output characteristic curve is shown in Fig. 4*a*. The transistor performance can be evaluated by figure-of-merit mobility. The electron mobility indicates how fast charge carriers move inside the material. Electron mobility directly related to current driving capability and resulting circuit speed. The electrical characteristic of the phototransistor in the linear region ($V_{gs} \gg V_{ds}$) is derived from the following expression:

$$I_{ds} = \frac{\mu w C_{ox}}{l}\left(V_{gs} - V_t\right)V_{ds} \tag{1}$$

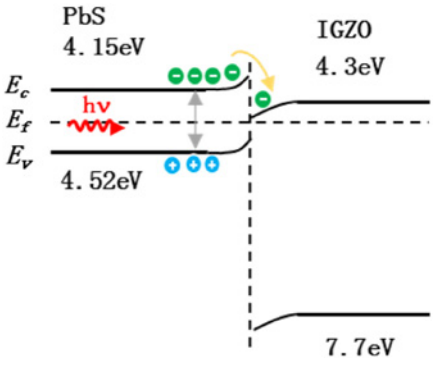

Fig. 1 *Energy band diagram of the IGZO/PbS interface*

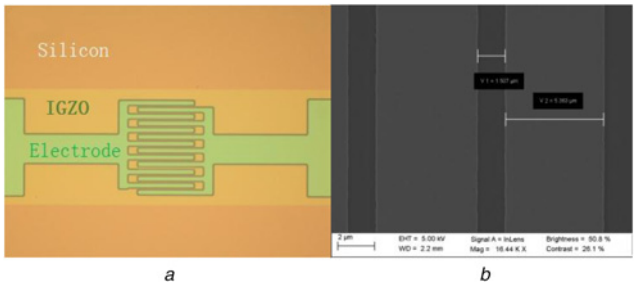

Fig. 2 *Surface image analysis of transistor*
a Microstructure image of the single transistor
b SEM images of the sample of discontinuous PbS thin films

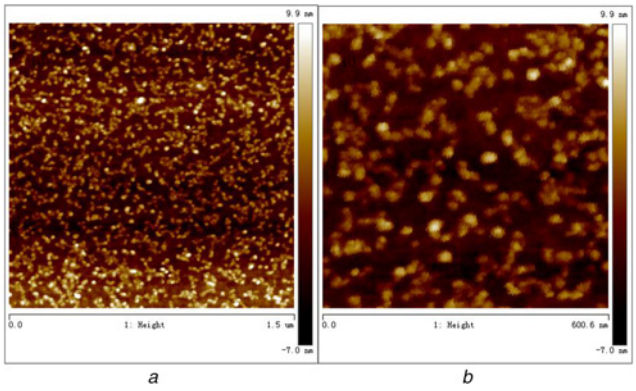

Fig. 3 *AFM images of PbS thin films deposited with thickness of 1 nm in different ruler scales*
a AFM images of PbS thin films in ruler scales of 0–1.5 μm
b AFM images of PbS thin films in ruler scales of 0–0.6 μm

where I_{ds} is the drain current, μ is electron mobility, w is the width of electrode and l is the length of electrode, C_{ox} is the capacitance per unit area of the insulation layer, V_t is the threshold voltage, V_{gs} is the gate voltage. The capacitance per unit area of the insulation layer is calculated by

$$C_{ox} = \frac{\varepsilon_0 \varepsilon_r}{t_{ox}} \tag{2}$$

with $\varepsilon_{r(SiO2)} = 3.9$, where $t_{ox} = 300$ nm is the thickness of insulation layer. Meanwhile, the electron mobility and gate voltage could be extracted with the following relationship:

$$\mu = \frac{l}{V_{ds} C_{ox} w}\frac{\partial I_{ds}}{\partial V_{gs}} \tag{3}$$

According to the formula, the mobility of electron transport layer could reach 28.9 $cm^2V^{-1}s^{-1}$ when transistor only deposited IGZO, and the electron mobility of transistor could reach 8.7 $cm^2V^{-1}s^{-1}$ after deposited PbS. Compared with similar PbS phototransistors, the mobility of this device has been greatly improved [15–18]. The subthreshold swing (ss) of the device is the gate voltage increment required to change the leakage current by an order of magnitude. It is reflecting the interface state density and defects to some extent. The ss is defined as follows:

$$\mathrm{ss} = \frac{\partial V_{gs}}{\partial\left(\log I_{ds}\right)} \tag{4}$$

Fig. 4*b* depicts contrast of initial (without annealed) and annealed of transfer characteristic. The device was placed on a heating station and annealed at 300°C for 30 min in the air environment.

It can increase the oxygen ion in electron transport layer when it is annealed in the air, which in turn makes the threshold voltage positive shift, and improve the performance of device. Compared with the performance of non-annealed phototransistor, the subthreshold swing of the device reduced to 0.60 V/dec. Threshold voltage approximately shifted forward by 15 V. Fig. 4*c* shows the hysteresis curves for PbS/IGZO TFTs in saturation [19]. As shown in Fig. 4*c*, the TFT dark on/off current ratio is larger than 10^9 with low hysteresis (ΔV ~1.8 V, where ΔV is the subthreshold characteristic shift) during measurements.

3.3. Optical properties: Fig. 5*a* shows power-dependent field effect transfer curves under various illumination intensities of $P = 1.61$ nW, 4.66 nW, 8.95 nW, 13.2 nW [20], which uses the

doi: 10.1049/mnl.2018.5249

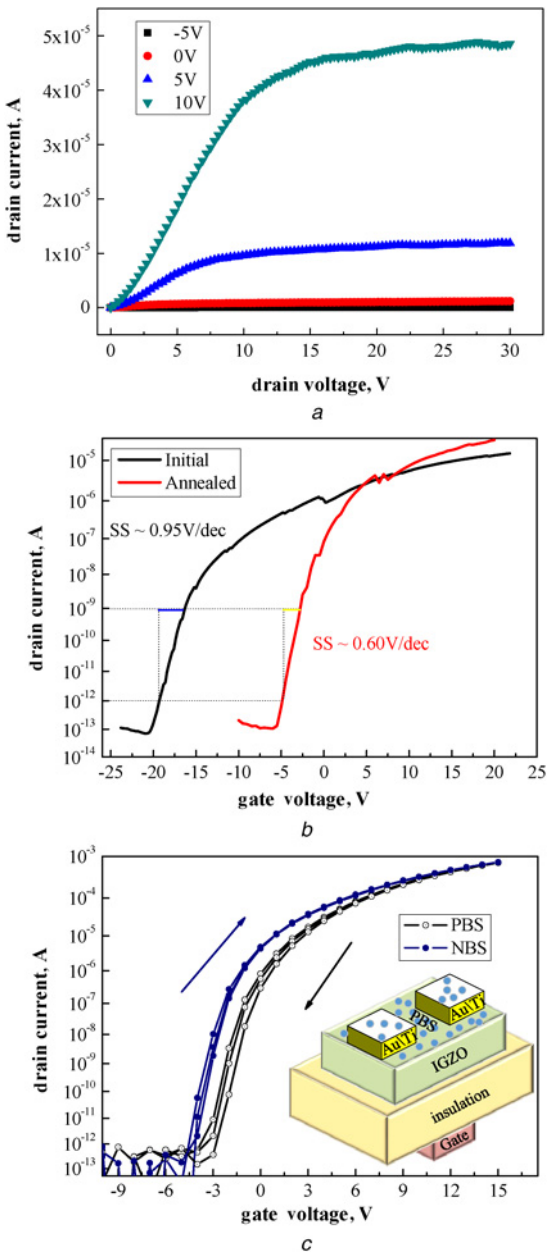

Fig. 4 *Devices performance in dark at room temperature*
a TFT output characteristic. Inset image is the schematic diagram of the transistor
b Contrast of initial and annealed transfer characteristic curves
c Hysteresis curves for PbS/IGZO TFTs in saturation, the bule line was tests in positive bias stress (PBS) and the dark line was tests in negative bias stress (NBS)

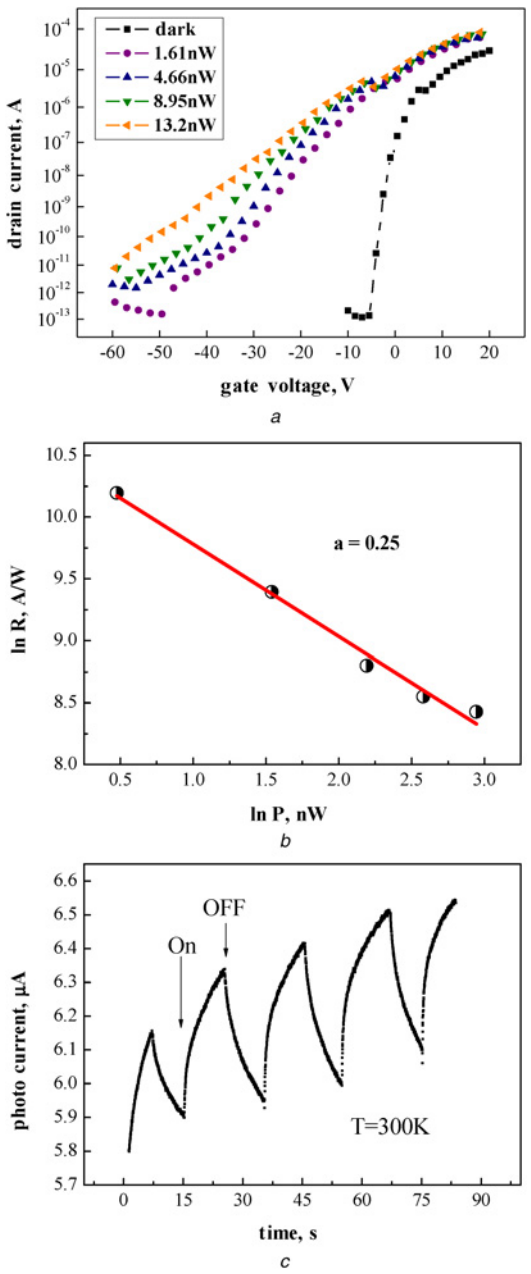

Fig. 5 *Results of using the pumped light with the wavelength of 532 nm*
a Power-dependent field effect transfer curves
b Light- power dependency of responsivity for devices, simulated with power law, $R \sim P^{\alpha-1}$
c Time-resolved photocurrent rise and decay after switching on and off the 532 nm laser illumination under vacuum conditions

pumped light with the wavelength of 532 nm. The sensitivity of the phototransitor is the ratio of photo-dark current. As we can see in Fig. 5*a*, the sensitivity up to 10^7 from the dark to illumination when $V_g = -3$ V. Furthermore, we obtained a remarkable high on/off current (I_{on}/I_{off}) ratio of 10^8 without illumination under the condition of bias at 1 V. These performance parameters are satisfying compared with other reported thin film heterojunction transistors under the similar conditions [21]. As we all know, photoresponsivity (R) is a key factor to identify the light-sensitive performance of phototransistor. The responsivity as a function of the illumination wavelength can be evaluated via the following equation:

$$R = \frac{I_{ph}}{P} = \frac{I_{\text{light}} - I_{\text{dark}}}{P} \tag{5}$$

where I_{ph} is the difference current of dark field to light field, P is the incident optical power at which the devices are illuminated, I_{dark} is the drain current under no illumination and I_{light} is the drain current when exposed to laser [22]. The I_{ph} suggests that the response performance is closely related to electron mobility. Responsivity could reach up to 2.7×10^4 A/W at $P = 1.61$ nW when I_{ph} is 4.31×10^{-5} A, which are more satisfied. Light-power dependence of responsivity simulated with power law: $R \propto P^{\alpha-1}$. The value of α ranges from 0 to 1, reflecting the degree of lost photo-excited carriers through recombination [23]. As shown in Fig. 5*b*, the optical power dependency of responsivity value is plotted in logarithmic coordinates. In this work, a linear fit between ln R and ln P reveals the α of 0.25, which indicates that photo-generated electron–hole pairs are effectively separated. Another important parameter of a transistor is the specific detectivity. We refer to Eun Kyu

Kim's method [9], assuming that shot noise from dark current is the main contribution in detection assessment, the detectivity(D^*) is given by the following equation:

$$D^* = \frac{R}{\sqrt{2eI_{\text{dark}}/A}} \tag{6}$$

Here, e is the elementary charge and A is the effective area of the phototransistor. The photosensitivity of the PbS/IGZO phototransistor rapidly increased with illumination, and a high detectivity of 2.97×10^{13} cmHz$^{1/2}$W^{-1} was obtained at the power intensity of 0.136 mW cm^{-2} when $\lambda = 532$ nm. Fig. 5*c* shows the time-resolved photocurrent rise and decay after switching on and off the 532 nm laser illumination under vacuum conditions ($V_g = 7$ V; $V_{ds} = 1$ V). As we know, electron–hole pairs could be generated through trap-assisted emission under the condition of light illumination. The photocurrent increases and V_t shifts negatively when the device was exposed to light, and the rise time is ~3.8 s. V_t moves positively when the light is turned off, and the recovery time was ~8.0 s, which was much higher than rise time. In addition, the saturation current of each cycle is also increasing. In depletion mode of TFT, a possible generation of oxygen vacancy (OV) results in the positive hole, constituting a deep acceptor. It describes an OV acting by using a Kroger-Vink notation as follows [24]:

$$V_o^x \rightarrow V_o^{\cdot\cdot} + 2e^- \tag{7}$$

The V and O stand for vacancy and oxygen atom neutral, while the superscripts 'x' and '$\cdot\cdot$' represent neutral and negative charge states, respectively. One possible reason is that the energy of the photons will induce the generation of OV and help the oxygen atoms (O_{atom}) in the active layer to diffuse to the interstitial sites. This process can be described by the following:

$$V_o^{\cdot\cdot} \rightarrow O_{\text{atom}} + 2e^- \tag{8}$$

After turning off the light, the gap oxygen atoms require relatively high energy to overcome the barriers of the surrounding ions for diffusing back into the lattice position [25]. So, it takes some time for the system to return to the initial pre-illumination state. Even that, a relatively shorter response time has been obtained in this work [23, 26]. Moreover, another power-dependent field-effect transfer curves using the pumped light with the wavelength of 808 nm also was taken in different light power. As shown in Fig. 5*a*, the sensitivity up to 10^6 from the dark to illumination when $V_g = -5$ V. Furthermore, we obtained a remarkable high I_{on}/I_{off} ratio of 10^9 without illumination under the condition of bias at 1 V. Fig. 6*b* also presents optical power dependency of responsivity value, the responsivity could reach up to 5.7 A/W at $P = 0.6$ µW when I_{ph} is 3.42×10^{-6} A. It reveals α as 0.47 by a linear fit between ln R and ln P. This is also a satisfactory value for our phototransistor.

3.4. Diode properties: A source–drain diode (body diode) of the field-effect transistor (FET) was used as a freewheeling diode. This body diode can therefore be utilised to conduct current through the power FET structure in the third quadrant of operation. To reduce the cost and packaging complexity, it is attractive to use the integral body diode within the power FET structure instead of a separate antiparallel fly-back diode [27]. In this Letter, we studied the I–V characteristics of body diodes in dark and light conditions, respectively. We test the source–drain I–V characteristics of the body diode under the condition of $V_{gs} = 0$. There are two back-to-back junctions created between the source, base and drain regions in the FET structure. In order to suppress the parasitic transistor, the junction (J_1) between the source and base region is always short-circuited [27]. Consequently, the FET can only

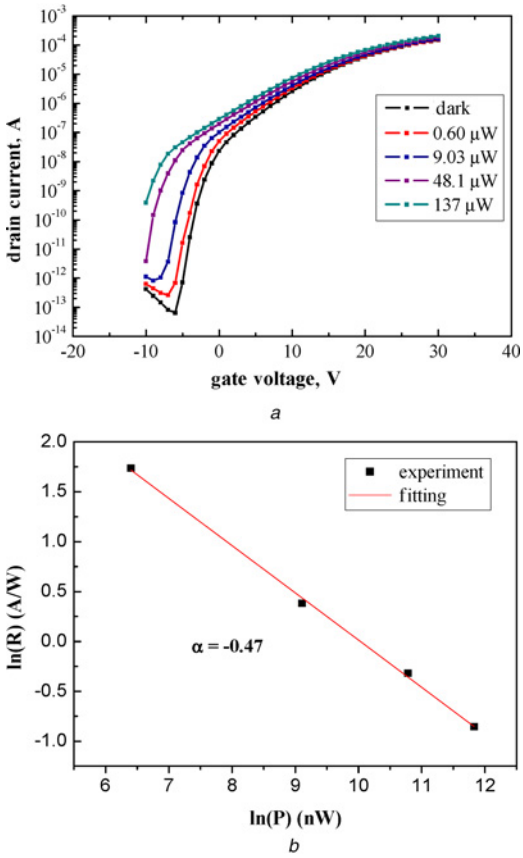

Fig. 6 *Results of using the pumped light with the wavelength of 808 nm*
a Power-dependent field effect transfer curves
b Light-power dependency of responsivity for devices, simulated with power law, $R \sim P^{\alpha-1}$

support a high voltage in the first quadrant of operation ($V > 0$), and the I–V characteristics resemble for a resistor. The light power-controlled drain current will be saturated when the drain bias voltages approach and exceed the gate bias (the illumination produces heat-balanced electrons, which is equivalent to increasing the gate voltage). However, the junction (J_2) between the base region and the drift region becomes forward biased when a negative bias ($V < 0$) is applied to the drain terminal, as shown in Fig. 7*a*. In negative bias, current flow can occur between the drain and source electrodes, because the source electrode is also connected to the base region in the FET structure to suppress the parasitic transistor. This is referred to as the current flow through the body diode of the transistor. The body diode current characteristics in dark is shown in the inset of Fig. 7*a*. It is possible to induce larger drain current flow at low negative drain bias voltages by the application of light.

This current flow occurs via the channel in the FET structure whose resistance determines the on-state voltage drop in the third quadrant. The current characteristics can be described by the p-n junction I–V equation:

$$I_d = I_s\left(\exp\left(\frac{eV}{kT}\right) - 1\right) \tag{9}$$

I_s is the saturation current. As shown in inset image, we estimated the saturation current is about 0.422 nA in dark condition. Fig. 7*b* shows the photo-responsivity curves of both the transistor (dark curves) and body diode (red curve). For transistors, the responsivity can be well regulated by the gate voltage when the laser power is

doi: 10.1049/mnl.2018.5249

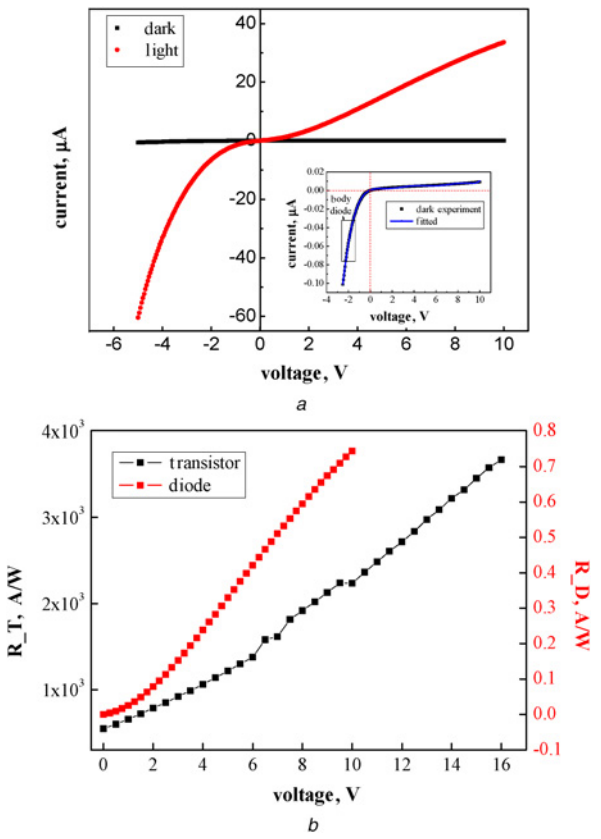

Fig. 7 Results of diode properties
a Field transistor characteristics in the third quadrant in dark and light; inset image is the *I–V* characteristics in dark
b Photoresponsivity curves of the device under the tunable of gate voltage

1.61 nW. For body diodes, the photo-responsivity can also be adjusted by the drain bias voltage when the optical power is 0.113 mW. It gets an optical response of ∼0.74 A/W at the bias of 16 V. This result is also satisfactory in current diode phototransistor [28].

4. Conclusion: In conclusion, a discontinuous PbS thin film was successfully prepared to form a hybrid back-gate phototransistor combined amorphous IGZO. The photo-sensitive layer was prepared by a PVD conveniently. More importantly, a thermal deposition method is used to prepare a thin film lead sulphide in the air without passivation to fabricate a device which shows excellent stability. The IGZO was used as channel of TFT because it has high mobility and well gate tunable ability. The fabricated phototransistor has a high mobility of 8.7 $cm^2V^{-1}s^{-1}$, which is much better than traditional PbS TFTs. The phototransistor has a high responsivity of 2.7×10^4 A/W, and high on/off current ratio of 10^8 in visible spectrum. It also has satisfactory properties in the near infrared spectrum. The responsivity is 5.7 A/W, and the on/off current ratio as high as 10^9 in near-infrared spectrum, respectively. In addition, the body diode shows good characteristics with saturation current as small as 0.422 nA, and the optical response is ∼0.74 A/W. This phototransistor can be further applied in the fields of intelligent housing system active-matrix flat-panel displays and environmental monitoring.

5. Acknowledgments: This work was supported by the National Natural Science Foundation of China (grant nos. 61335008, 61601455), National High Technology Research and Development Program of China (grant no. 2015AA042605).

6 References

[1] Gao L., Dong D.D., He J.G., *ET AL.*: 'Wearable and sensitive heart-rate detectors based on PbS quantum dot and multiwalled carbon nanotube blend film', *Appl. Phys. Lett.*, 2014, **105**, p. 153702
[2] Someya T., Iba S., Kato Y., *ET AL.*: 'A large-area, flexible, and lightweight sheet image scanner integrated with organic field-effect transistors and organic photodiodes'. 50th IEEE International Electron Devices Meeting, San Francisco, CA, USA, 2004, pp. 365–368
[3] Han S.Y., Jeon K.S., Song J., *ET AL.*: 'Photo-related stress effects in a-SiGe: H thin film transistors for infrared image sensors', *J. Disp. Technol.*, 2013, **9**, pp. 30–36
[4] Chuang C.S., Fung T.C., Mullins B.G., *ET AL.*: 'Photosensitivity of amorphous IGZO TFTs for active-matrix flat-panel displays'. International Symposium of the Society-for-Information-Display, Los Angeles, CA, USA, 2008, pp. 1215–1218
[5] Stepanov E.V., Kouznetsov A.I.: 'Multicomponent fiber-optical gas sensor based on MIR tunable diode lasers', *Infrared Phys. Technol.*, 1996, **37**, pp. 149–153
[6] Atsushi K., Hideki M., Mitsuhisa I., *ET AL.*: 'Memory operation of oilicon quantum-dot floating-gate metal-oxide-semiconductor field-effect transistors', *Jpn. Soc. Appl. Phys.*, 2001, **40**, pp. L721–L723
[7] Su W.C., Chang T.C., Liao P.Y., *ET AL.*: 'The effect of asymmetrical electrode form after negative bias illuminated stress in amorphous IGZO thin film transistors', *Appl. Phys. Lett.*, 2017, **110**, p. 103502
[8] Hays D.C., Gila B.P., Pearton S.J., *ET AL.*: 'Energy band offsets of dielectrics on $InGaZnO_4$', *Appl. Phys. Rev.*, 2017, **4**, p. 021301
[9] Pak S.W., Chu D., Song D.Y., *ET AL.*: 'Enhancement of near-infrared detectability from InGaZnO thin film transistor with MoS_2 light absorbing layer', *Nanotechnology*, 2017, **28**, p. 11203
[10] Hwang D.K., Lee Y.T., Lee H.S., *ET AL.*: 'Ultrasensitive PbS quantum-dot-sensitized InGaZnO hybrid photoinverter for near-infrared detection and imaging with high photogain', *NPG Asia Mater.*, 2016, **8**, p. E233
[11] Zhang H.T., Zhang Y.T., Song X.X., *ET AL.*: 'The ambipolar operation of lateral and vertical PbSe quantum dots field effect phototransistors'. 8th International Symposium on Advanced Optical Manufacturing and Testing Technologies (AOMATT) – Optoelectronic Materials and Devices, Suzhou, China, 2016, p. 96860
[12] Prins F., Buscema M., Seldenthuis J.S., *ET AL.*: 'Fast and efficient photodetection in nanoscale quantum-dot junctions', *Nano Lett.*, 2012, **12**, pp. 5740–5743
[13] Pennebaker W.B.: 'PbS thin film transistors', *Solid-State Electron.*, 1965, **8**, pp. 509–515
[14] Fung T.C., Chuang C.S., Chen C., *ET AL.*: 'Two-dimensional numerical simulation of radio frequency sputter amorphous In–Ga–Zn–O thin-film transistors', *J. Appl. Phys.*, 2009, **106**, p. 084511
[15] Dogan S., Bielewicz T., Cai Y., *ET AL.*: 'Field–effect transistors made of individual colloidal PbS nanosheets', *Appl. Phys. Lett.*, 2012, **101**, p. 073102
[16] So H., Choi H., Shim H.C., *ET AL.*: 'Atomic layer deposition effect on the electrical properties of Al_2O_3-passivated PbS quantum dot field-effect transistors', *Appl. Phys. Lett.*, 2015, **106**, p. 093507
[17] Jo C.H., Kim J.H., Kim J., *ET AL.*: 'Low-temperature annealed PbS quantum dot films for scalable and flexible ambipolar thin-film-transistors and circuits', *J. Mater. Chem. C*, 2014, **2**, (48), pp. 10305–10311
[18] Morales-Fernandez I.E., Medina-Montes M.I., Gonzalez L.A., *ET AL.*: 'Electrical behavior of p-type PbS-based metal-oxide-semiconductor thin film transistors', *Thin Solid Films*, 2010, **519**, pp. 512–516
[19] Yao J., Xu N.S., Deng S.Z., *ET AL.*: 'Electrical and photosensitive characteristics of a-IGZO TFTs related to oxygen vacancy', *IEEE Trans. Electron Devices*, 2011, **58**, (4), pp. 1121–1126
[20] Meng Y., Wang J.W., Ming A.J., *ET AL.*: 'A novel PbS/n-IGZO thin-film nano-photodetector with high responsivity and high photo-to-dark current ratio'. 13th IEEE NEMS, Singapore, Singapore, 2018
[21] Mi L.F., Yu Y.Q., Wang H., *ET AL.*: 'Ultrasensitive PbS-quantum-dot photodetectors for visible-near-infrared light through surface atomic-ligand exchange', *Part. Part. Syst. Charact.*, 2015, **32**, (12), pp. 1102–1109

[22] Wang J.W., Liu F.J., Wang G.T., *ET AL.*: 'Novel organic-perovskite hybrid structure forward photo field effect transistor', *Org. Electron.*, 2016, **38**, pp. 158–163
[23] Zhang W.J., Huang J.K., Chen C.H., *ET AL.*: 'High-gain phototransistors based on a CVD MoS(2) monolayer', *Adv. Mater.*, 2013, **25**, (25), pp. 3456–3461
[24] Kofstad P.: 'Nonstoichiometry, diffusion, and electrical conductivity in binary metal oxides' (Wiley-Interscience, New York, NY, USA, 1972)
[25] Takechi K., Nakata M.N., Eguachi T., *ET AL.*: 'Comparison of ultraviolet photo-field effects between hydrogenated amorphous silicon and amorphous $InGaZnO_4$ thin-film transistors', *Jpn. J. Appl. Phys.*, 2009, **48**, (1), p. 010203
[26] Studenikin S.A., Golego N., Cocivera M.: 'Carrier mobility and density contributions to photoconductivity transients in polycrystalline ZnO films', *J. Appl. Phys.*, 2000, **87**, (5), pp. 2413–2421
[27] Jayant Baliga B.: 'Fundamentals of power semiconductor devices' (Springer Science + Business Media, New York, NY, USA, 2008)
[28] Sara-nr R., Curry R.J.: 'Lead sulphide nanocrystal photodetector technologies', *Nat. Photonics*, 2016, **10**, (2), pp. 81–92

doi: 10.1049/mnl.2018.5249